

Structure of acetylcholinesterase complexed with E2020 (Aricept®): implications for the design of new anti-Alzheimer drugs

Gitay Kryger^{1*}, Israel Silman² and Joel L Sussman^{1,3}

Background: Several cholinesterase inhibitors are either being utilized for symptomatic treatment of Alzheimer's disease or are in advanced clinical trials. E2020, marketed as Aricept®, is a member of a large family of *N*-benzylpiperidine-based acetylcholinesterase (AChE) inhibitors developed, synthesized and evaluated by the Eisai Company in Japan. These inhibitors were designed on the basis of QSAR studies, prior to elucidation of the three-dimensional structure of *Torpedo californica* AChE (*TcAChE*). It significantly enhances performance in animal models of cholinergic hypofunction and has a high affinity for AChE, binding to both electric eel and mouse AChE in the nanomolar range.

Results: Our experimental structure of the E2020–*TcAChE* complex pinpoints specific interactions responsible for the high affinity and selectivity demonstrated previously. It shows that E2020 has a unique orientation along the active-site gorge, extending from the anionic subsite of the active site, at the bottom, to the peripheral anionic site, at the top, via aromatic stacking interactions with conserved aromatic acid residues. E2020 does not, however, interact directly with either the catalytic triad or the 'oxyanion hole', but only indirectly via solvent molecules.

Conclusions: Our study shows, *a posteriori*, that the design of E2020 took advantage of several important features of the active-site gorge of AChE to produce a drug with both high affinity for AChE and a high degree of selectivity for AChE versus butyrylcholinesterase (BChE). It also delineates voids within the gorge that are not occupied by E2020 and could provide sites for potential modification of E2020 to produce drugs with improved pharmacological profiles.

Introduction

Observations documenting adverse effects of anticholinergic drugs on memory [1], taken together with postmortem data that revealed low cholinergic activities in Alzheimer's disease (AD) patients [2], led to the hypothesis, known as the 'cholinergic hypothesis', that AD is associated with an impairment in cholinergic transmission [3–5]. This led to the suggestion that cholinesterase (ChE) inhibitors would reverse a putative deficit in acetylcholine (ACh) levels associated with AD, and thus might reverse the memory impairments characteristic of the disease [5,6]. Consequently, a number of ChE inhibitors have been considered as candidates for the symptomatic treatment of AD and have been utilized in clinical trials. They include natural substances, such as physostigmine [6] and huperzine A [7], both of which are alkaloids, and synthetic compounds such as SDZ ENA-713, also known as Exelon® [8], and metrifonate [9]. Recently, evidence was presented that acetylcholinesterase (AChE) accelerates assembly of amyloid- β -peptides into the amyloid fibrils that form the senile plaques characteristic of AD [10]. It was suggested that a hydrophobic environment close to the peripheral binding site of the enzyme, at or near the entrance to the active-site gorge, might be involved in this process [11].

Addresses: ¹Department of Structural Biology, Weizmann Institute of Science, Rehovot 76100, Israel, ²Department of Neurobiology, Weizmann Institute of Science, Rehovot 76100, Israel and ³Department of Biology, Brookhaven National Laboratory, Upton, NY 11972, USA.

*Corresponding author.
E-mail: Gitay.Kryger@Weizmann.ac.il

Key words: acetylcholinesterase, Alzheimer's disease, crystal structure, drug–protein complex

Received: 18 November 1998
Revisions requested: 15 December 1998
Revisions received: 23 December 1998
Accepted: 11 January 1999

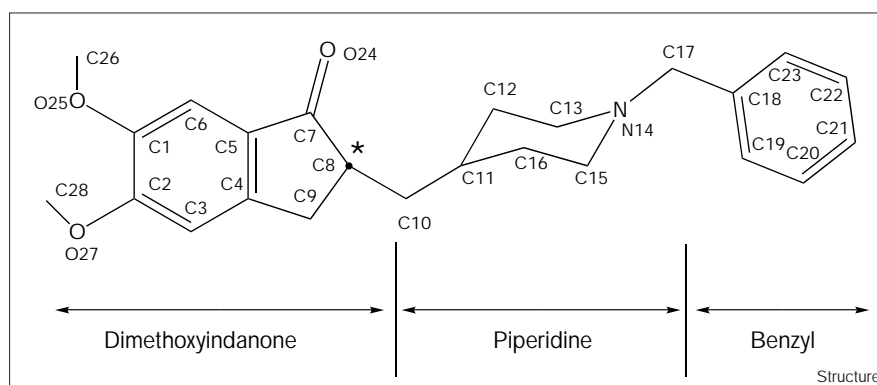
Published: 1 March 1999

Structure March 1999, 7:297–307
<http://biomednet.com/elecref/0969212600700297>

© Elsevier Science Ltd ISSN 0969-2126

The first, and thus far the only, two drugs approved by the United States Food and Drug Administration (FDA) for treatment of AD are both reversible inhibitors of AChE. They are tacrine (THA), approved in 1993 and marketed as Cognex® [12], and the more potent ChE inhibitor, E2020 ((*R,S*)-1-benzyl-4-[(5,6-dimethoxy-1-indanon)-2-yl]methylpiperidine; Figure 1), also known by its trivial name donepezil hydrochloride and marketed as Aricept®, which was approved in 1996 [13]. E2020 is a member of a large family of *N*-benzylpiperidine-based AChE inhibitors that were developed, synthesized and evaluated by the Eisai Company in Japan [14], on the basis of QSAR studies [15,16], prior to elucidation of the three-dimensional (3D) structure of *Torpedo californica* AChE (*TcAChE*) [17]. It was shown to significantly enhance performance in animal models of cholinergic hypofunction [18], and to have high affinity for AChE, binding to both electric eel and mouse AChE in the nanomolar range [19]. THA and E2020 share the same target, but whereas THA must be administered up to four times a day, and is associated with hepatotoxicity, slow pharmacokinetics and a high incidence of side effects, E2020 offers the patient significant improvements by being administered only once a day and having fewer side effects. Furthermore, E2020 displays high selectivity for AChE in

Figure 1



comparison to butyrylcholinesterase (BChE); this may be important, as it has been suggested that inhibition of BChE, which is abundant in human plasma, may cause potentiating side effects [20,21]. The affinity of E2020 for human AChE is ~1000-fold greater than for human BChE, whereas THA has a similar affinity for the two enzymes [22,23].

Attempts to explain the specificity of E2020, and of other Eisai inhibitors, were made originally using QSAR and by theoretical conformational analysis. Subsequent to determination of the 3D structure of *Tc*AChE, automated computational techniques based on the known coordinates were employed [24,25]. Although the earlier modeling studies attributed the differential specificity for AChE and BChE to differences in the geometry within the active site [26], the more recent studies suggested that E2020 and the other Eisai compounds are oriented along the axis of the active-site gorge and that the differential specificity can be attributed to structural differences in AChE and BChE at the top of the gorge, at the 'peripheral' anionic site [14,24,25]. Our experimental structure of the E2020-*Tc*AChE complex broadly confirms these latter assignments and pinpoints the specific interactions that are responsible for the high affinity and selectivity demonstrated previously.

Results and discussion

Overall structure

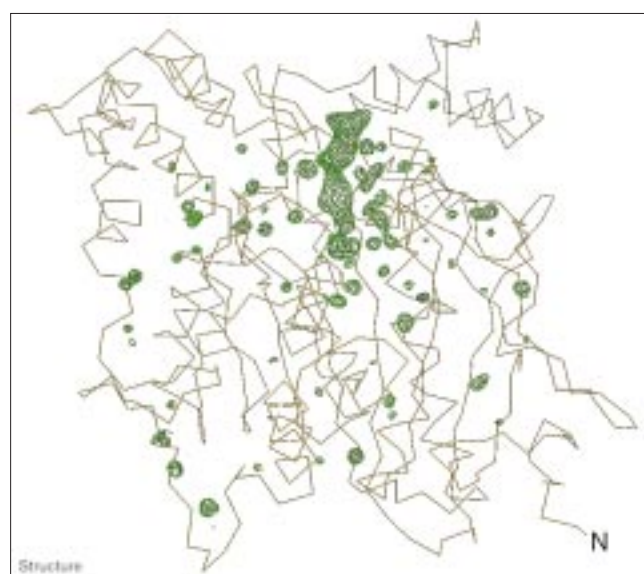
The overall structure of the E2020-*Tc*AChE complex at 2.5 Å resolution is shown in Figure 2. The protein is displayed as a coil with the initial difference electron-density map of E2020 superimposed as a 'chicken-wire' net. It can be clearly seen that E2020 has a unique orientation along the active-site gorge, extending from the anionic subsite of the active site, at the bottom near Trp84, to the peripheral anionic site, at the top near Trp279 (see Figures 3 and 4). The 3D structure of the complex shows more detail of the AChE structure than the starting native model (Protein Data Bank [PDB] code 2ACE). Specifically, residues 2 and 3, at the N terminus, and the 484-490 loop, which were not seen in the original model, can be discerned. In

addition, it was possible to model the proximal *N*-acetylglucosamine (NAG) moiety at four out of five putative glycosylation sites [27], namely at residues Asn59, Asn416 (where two moieties could be fitted), Asn457 and Asn533. An analysis of the quality of the refined model is summarized in Table 1.

All three segments of E2020 interact with AChE

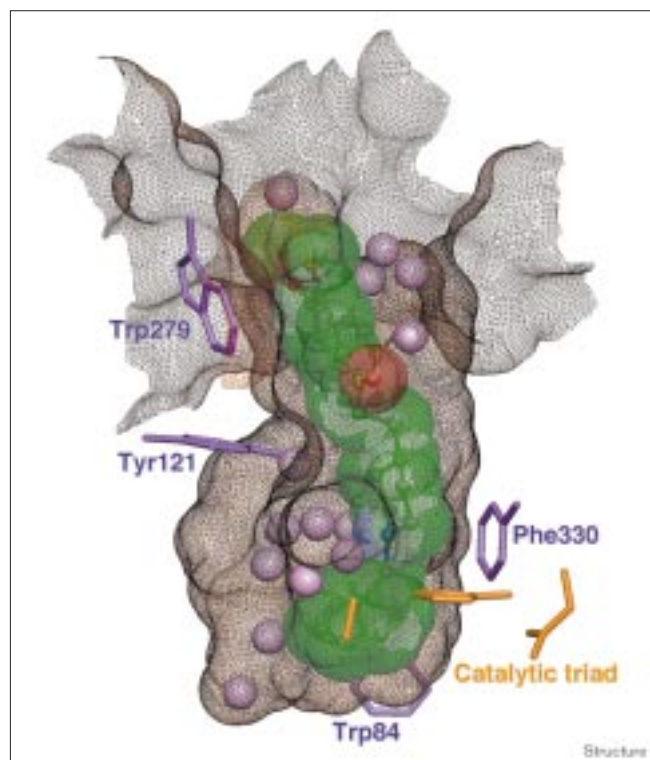
As seen in Figure 5, E2020 makes principal interactions along the active-site gorge of the enzyme through its three major functional groups: the benzyl moiety, the piperidine nitrogen, and the dimethoxyindanone moiety. These interactions involve discrete water-mediated contacts that seem to be crucial for binding and specificity.

Figure 2



Initial difference electron-density map, contoured at 4.5σ , based on the native *Tc*AChE structure (PDB code 2ACE) and the diffraction data for the E2020-*Tc*AChE complex.

Figure 3



E2020 binds along the active site and interacts with the ‘peripheral anionic’ subsite at the top and with the ‘anionic’ subsite at the bottom. E2020 is displayed in green semi-transparent CPK and ball-and-stick representation, solvent molecules are shown as lilac balls, catalytic triad residues are in orange, binding residues are shown as purple sticks, and the solvent-accessible surface of the gorge is shown as a brown net.

Interactions at the bottom of the gorge

Near the bottom of the gorge, one face of the benzyl ring displays classic parallel π - π stacking with the six-membered ring of the Trp84 indole, similar to the interaction with THA [28]. It thus occupies the binding site for quaternary ligands [28,29], which was also modeled for the quaternary group of the natural substrate, ACh [17,26]. The ring-to-ring distances range from 3.7 Å between Trp84 C δ 2 and E2020 C19 to 4.4 Å between Trp84 C ϵ 2 and E2020 C22.

On the opposite face, the benzyl group makes a classic aromatic hydrogen bond (H bond) [30,31] with a water molecule (WAT 1160), with distances to the ring carbons of 3.5 Å–3.7 Å. This solvent molecule is held firmly, as assessed by a below-average temperature factor, by an H bond to another solvent molecule (WAT 1161) in the ‘oxanion hole’ and to WAT 1159 (see below). WAT 1161 is another example of a tightly bound water molecule with a relatively low temperature factor; it makes an H bond with the residues of the oxanion hole, namely with Gly118 N, Gly119 N and Gly201 N, as well as with

Figure 4



The E2020–*TcAChE* complex. Ribbon diagram showing the complex of the drug bound to the enzyme.

Ser200 O γ . Finally, the kinetic evidence showing that E2020 binds to the free and the acylated forms of AChE [32] is corroborated by our observation that E2020 does not interact with the catalytic triad. Other interactions are shown schematically in Figure 5.

Interactions in the middle of the gorge

In the constricted region, halfway up the gorge (Figures 3 and 4), the charged nitrogen of the piperidine ring makes a cation- π interaction [33,34] with the phenyl ring of Phe330, with distances of 3.9 Å–4.5 Å between the nitrogen and the ring carbons. The orientation of the phenyl ring is similar to that seen in the complex of decamethonium (DECA) with *TcAChE* (DECA–*TcAChE*; PDB code 1ACL) [28]. The ring nitrogen also makes an in-line 2.9 Å H bond with WAT 1159, which, in turn, makes H bonds with Tyr121 OH, with WAT 1158 and with WAT 1160 (see above). As already mentioned, the binding site for the quaternary nitrogen of ACh, and for homologous ligands, is the indole ring of Trp84 [17,26,28]. These data suggest that Phe330 may serve as an additional quaternary binding site, midway down the gorge, between the peripheral site and the anionic subsite of the active site.

Interactions at the entrance to the gorge

At the top of the gorge the indanone ring stacks against the indole ring of Trp279, in the peripheral binding site, by a classical π - π interaction. Specifically, E2020 C1, C2, C6, O25, C26, O27 and C28 stack against the six-membered ring of Trp279, with distances of 3.7 Å–4.2 Å. WAT 1249 lies in the plane of the indanone moiety, and H bonds to

Table 1

Data collection and refinement statistics.								
Data collection								
Detector	Raxis-II							
Source/wavelength (Å)	Rigaku FR300 (50 mA, 50 kV), 1.54184 (Cu K _α)							
Resolution range (Å)	30.0–2.5							
Number of reflections	34,264							
Completeness (%)	98.1							
Redundancy								
value	0	1	2	3	4	>5		
accumulated (%)	1.9	15.7	44.3	33.4	4.5	0.2		
<i>I</i> /σ								
value	0	1	2	3	5	10	20	>20
accumulated (%)	5.5	14.2	23.4	30.7	41.2	57.6	78.1	20.0
R _{sym} (%)	5							
Refinement								
Number of protein non-H atoms	4255 = 2137 mainchain + 2118 sidechain							
Number of hetero non-H atoms								
Water molecules	396							
Carbohydrate	70 = 5 × 14 in five NAG groups							
Inhibitor	28 in one E2020 group							
Resolution (Å)	2.5							
R _{work} (%)	18.8 (no σ cutoff)							
R _{free} (%)	22.9 (no σ cutoff)							
B factor (Å ²); Average / σ / Minimum / Maximum								
Protein	28.0 / 12.5 / 2.0 / 90.2							
Inhibitor	20.4 / 4.8 / 13.2 / 31.6							
Carbohydrate	47.6 / 15.0 / 14.5 / 74.5							
Water molecules	37.2 / 14.7 / 2.2 / 86.7							
Rmsd bond length (Å)	0.005							
Rmsd bond angle (°)	1.2							
Rmsd dihedral angle (°)	22.9							
Rmsd improper angle (°)	0.98							

$R_{\text{sym}} = \sum |I_i - \langle I \rangle| / \sum I_i$, $R_{\text{work}} = \sum ||F_o| - |F_c|| / \sum F_o$, R_{free} is calculated using 2000 random reflections.

the methoxy group of E2020 O25; it is also H-bonded to Glu185 Oε1 of the symmetry-related crystal-lattice copy of the enzyme. The carbonyl on the five-membered ring of the indanone only interacts with AChE via edge-on van der Waals contacts with the aromatic rings of Phe331 and Phe290. It also makes indirect contact, via WAT 1254, with Phe288 N. This finding might initially appear puzzling in view of the fact that a homolog of E2020, which lacks this carbonyl, was reported to be inactive [15]. Our structure-based suggestion is that the van der Waals contacts made by the carbonyl function help orient the indanone moiety to make a favorable interaction with the indole ring of Trp279. In the homolog which lacks this carbonyl function, the indanone moiety would be less constrained and would consequently make a poorer interaction with Trp279.

AChE selects the *R* form of E2020

The reported pharmacological studies on (*R,S*)-E2020 emphasize that both enantiomers are active; they have similar pharmacological profiles [22,32], but show ~fivefold difference in binding affinity for AChE: $K_i = 3.35$ nM (*R*), 17.5 nM (*S*) [32]. Although we used the racemate in our crystallographic study, we were not, therefore, surprised to see only the *R* form in the experimental electron-density

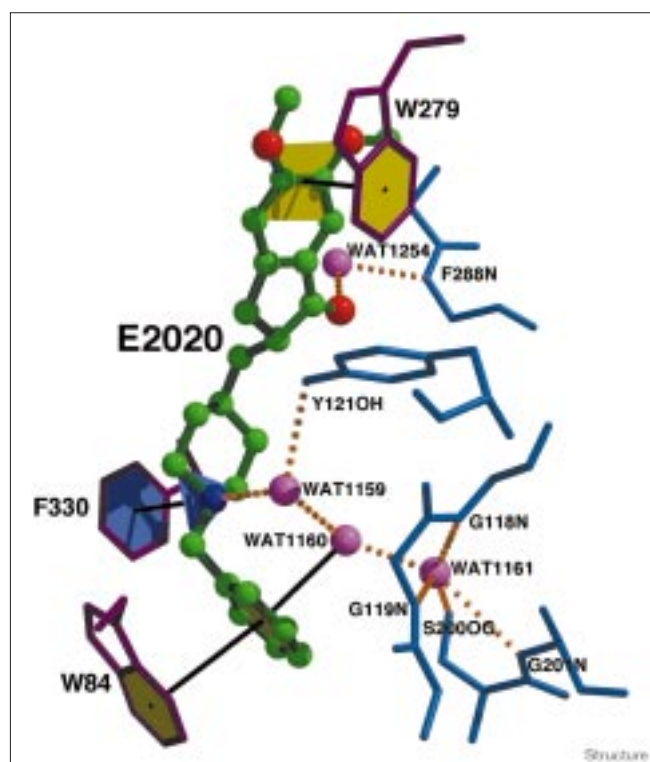
maps (see Figure 6). The observed conformation is very similar, if one allows for permitted adjustments of dihedral angles, to the energetically minimized E2020 conformation calculated with the InsightII package [35], and it is also similar to the 'small molecule' crystal structure of the pure *R* enantiomer (T Steiner, R Boer and J Kroon, personal communication).

E2020 analogs

Variation of the inhibitor backbone

Kawakami *et al.* [14] showed that at least two rotatable bonds on each side of the piperidine are needed to yield the high affinity displayed by E2020 and some of its analogs. We can now corroborate this observation by showing that the two aromatic moieties of E2020 interact closely with Trp84 and Trp279, while still maintaining the Phe330–piperidine–nitrogen interaction. This array of interactions calls for flexibility along the backbone of the inhibitor. The number of rotatable links is also important for optimal positioning of the aromatic systems of the inhibitor against their enzyme counterparts. Indeed, when two to three additional rotatable bonds are added between the indanone and the piperidine, affinity further increases (Table 2, lines 20–22), whereas adding rotatable bonds

Figure 5



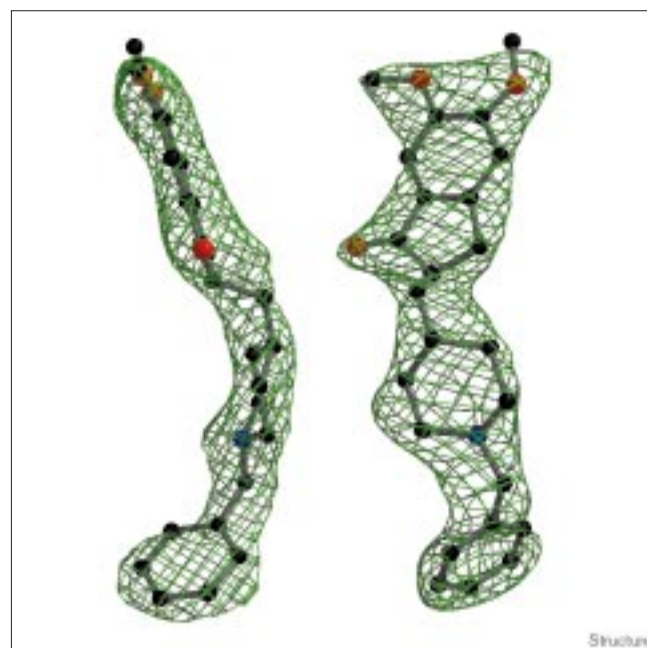
Major interactions between E2020 and TcAChE. Classical H bonds are shown as dashed lines, aromatic stacking and aromatic H bonds are shown as black lines connecting matching colored planes.

between the piperidine and the benzyl ring lowers it (Table 2, line 19). This distinction between adding rotatable bonds ‘above’ and ‘below’ the piperidine is likely to be based on the distances between Phe330 and either Trp84 or Trp279. Any change in the length of the spacer between Phe330 and Trp84 would weaken the interactions of the inhibitor with those sidechains. However, limited elongation of the indanone–piperidine link might allow more overlap of the indanone’s aromatic system with that of Trp279.

Variation of the benzyl moiety

E2020 is highly sensitive to substitutions on the benzyl moiety, as found by Kawakami and coworkers [14], who noticed a general preference for substitution at the *meta* (E2020 C20, C22) positions in comparison to the *ortho* (E2020 C19, C23) and *para* (E2020 C21) positions (see Table 2). Although these solution studies could not differentiate between the two possible *ortho/meta* substitutions, it can be seen from the crystal structure how each position would experience different environments with respect to the lining of the gorge and the structural solvent molecules within it. In general there is little space left between the benzyl ring and the gorge surface (Figures 3 and 4), which

Figure 6



Two views of E2020 modeled in the initial difference Fourier map. Only one enantiomer is observed in the crystal structure. The shape of the electron density around the chiral carbon and the carbonyl clearly resolve the *R/S* ambiguity. ‘Side’ and ‘front’ views of E2020 are shown modeled in the initial difference electron-density map contoured at 4.5σ .

may explain the sensitivity to substitutions of this moiety. The ring carbon at the *para* position is 3.2 \AA from Glu199 O ϵ 1; thus a substituent must be both small and able to make an H bond. Indeed, according to Kawakami *et al.* [14], an analogue with a hydroxyl at this position binds with higher affinity than the corresponding fluorine derivative (Table 2, lines 9–12). A substituent at the *meta* position, E2020 C22, will point to a very small space left between Glu199, His440 and Ser200 (the last two of which are members of the catalytic triad). The other *meta* position, at E2020 C20, points to a wider space partially bordered by Gly117 and the ‘oxyanion hole’. In our structure, this space is mostly occupied by solvent molecules and can accommodate a small, preferably negatively charged, substituent (Table 2, lines 5–7). A cyclohexane in place of a benzyl ring cannot make a π – π stacking interaction with Trp84, resulting in reduced affinity (Table 2, line 18).

Variation of the piperidine moiety

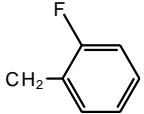
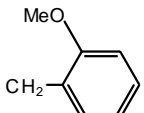
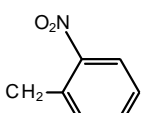
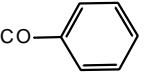
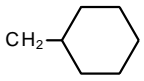
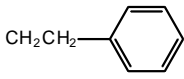
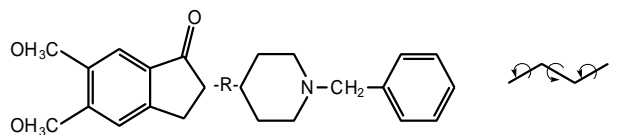

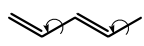
A piperazine in place of piperidine lowers the affinity of the resulting analog by ~ 19 -fold (Table 2, line 3), whereas a piperidine with a nitrogen at the opposite position (in place of E2020 C10) lowers the affinity by ~ 90 -fold (Table 2, line 2). A piperazine, although containing a nitrogen at a position suitable for binding with Phe330, possesses a different

Table 2

E2020 analogs.

Analog number	Constant	Variable R	Inhibition of AChE IC ₅₀ (nM) [14]
1.			5.7 (E2020)
2.			480
3.			94
4.			10
5.			1
6.			2
7.			4
8.			220
9.			1.8
10.			9.5
11.			40
12.			100

Table 2 continued

13.		9.5
14.		80
15.		160
16.		>10,000
17.	H	5400
18.		8.9
19.		180
20.		0.9
21.		1.5
22.		3.0

charge distribution, whereas a piperidine with a nitrogen at the opposite position does not allow a quaternary- π interaction with Phe330 to occur.

Variation of the indanone moiety

In general, substitutions on the indanone moiety have a smaller effect than substitutions on the benzyl group [15]. This is consistent with our crystal structure, as the indanone moiety is located in the wide section of the funnel-like

entrance to the gorge. Thus, some sites of substitution would point outwards towards the solvent, whereas others would point into the central region of the gorge. However, substitution on the same edge as the carbonyl group (C7 O24), which is juxtaposed to the wall of the gorge, would disrupt the parallel stacking to Trp279. This is consistent with the observation of Cardozo *et al.* [15] that a cyano substitution on E2020 C6 produces a relatively poor inhibitor. Suitable substitutions on the other edge of the

ring (namely E2020 C1, C2, C3 and C9) would be expected to have little effect or, possibly, result in improved affinity.

Comparison of the E2020–TcAChE complex with other complexes

The structures of native TcAChE and of six different complexes were overlaid according to their C α positions, namely native AChE (PDB code 2ACE) [36], and the complexes with tacrine (THA; PDB code 1ACJ) [28], DECA (PDB code 1ACL) [28], *m*-(*N,N,N*-trimethylammonio)trifluoroacetophenone (TMTFA; PDB code 1AMN) [29], huperzine (HUP; PDB code 1VOT) [36], edrophonium (EDR; PDB code 2ACK) and E2020 (PDB code 1EVE). Two issues arise from comparison of these structures: the role of Phe330, and the possible significance of structurally conserved solvent molecules within the gorge.

Phe330 as a 'swinging gate'

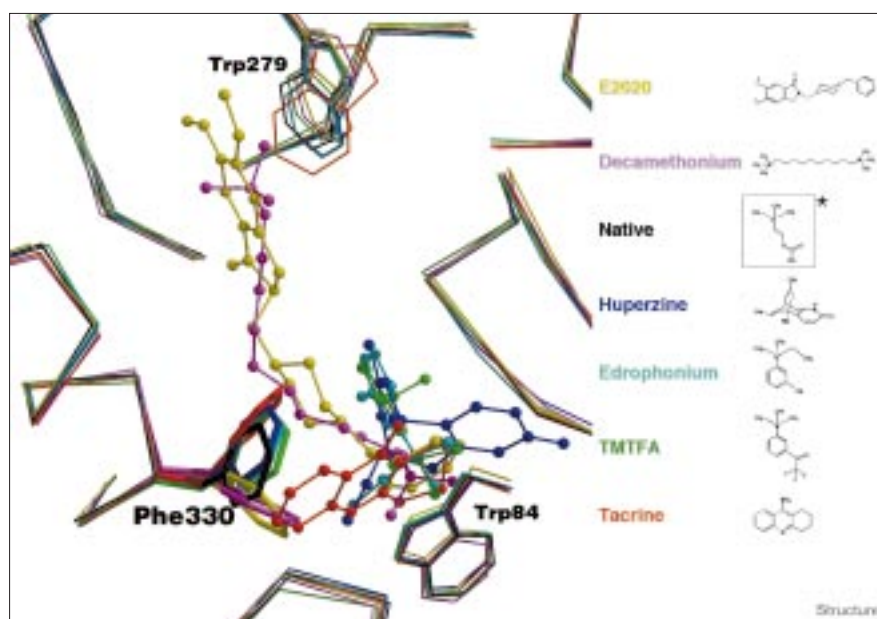
As seen in Figure 7, Phe330 adopts a wide range of conformations in the complex structures analyzed. These conformations can be assigned, primarily based on their χ_1 values, to three different groups. First, native, TMTFA, HUP and EDR ($\chi_1 = -162^\circ$, -174° , -171° and -177° , respectively). Second, THA ($\chi_1 = 157^\circ$). Third, E2020 and DECA ($\chi_1 = -130^\circ$ and -117° , respectively). In group 1, Phe330 adopts a similar conformation in the native enzyme and in the complexes with ligands that bind near the bottom of the gorge, with the exception of THA. This ligand defines Group 2, in which χ_1 and χ_2 of Phe330 change so as to permit its phenyl group to stack on top of the ligand, thus forming a 'sandwich' with the indole of Trp84. The common feature of Group 3 is the gorge-spanning ligand

that forces the aromatic ring of Phe 330 to swing out of the way towards the gorge wall. It is also of interest that the THA–TcAChE complex displays a different conformation for the indole group of Trp279 relative to native AChE and the other complexes (χ_2 value of 30° versus about 90° for the others). This provides some support for structural coupling along the gorge between the anion subsite of the active site and the peripheral anionic site, as suggested by Shafferman and coworkers [37]. The conformational flexibility displayed by the sidechain of Phe330, contrasted with the relative rigidity of the other sidechains lining the gorge, supports the notion that it contributes to the significantly higher catalytic activity of AChE relative to BChE, which lacks this residue. Site-directed mutagenesis studies [38,39] showed that elimination of this aromatic sidechain does not affect the K_m for both charged and uncharged ligands. It does, however, have a significant effect on k_{cat} , which decreases ~fourfold for cationic substrates, although it increases ~twofold for uncharged substrates. Thus, via the quaternary- π electron interaction clearly seen in the E2020 complex, it may serve to guide ACh towards the active site, while simultaneously isolating the reaction center from the rest of the gorge. In fact, substrate traffic down the gorge may actually occur concomitantly with a swinging movement of Phe330. Similar ideas have been proposed on the basis of molecular dynamics studies [40,41].

The solvent

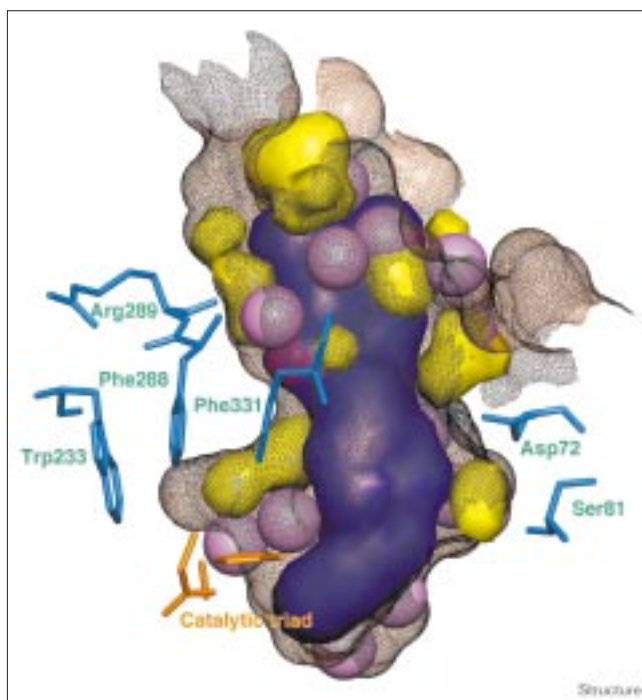
In the E2020–TcAChE complex, 25 ordered waters can be seen within the gorge. If one overlays this structure with that of the native enzyme and of five other complexes, as

Figure 7



Overlay of native TcAChE and six complexes. The flexibility of Phe330 in comparison with the rigidity of the rest of the gorge can be seen. Backbone trace and key residues are represented by thin lines, Phe330 by thick lines and inhibitors are shown in ball-and-stick representation. *A ChemDraw® representation of ACh is shown for purposes of comparison.

Figure 8



'Empty' spaces, where no ordered solvent molecule is observed, can accommodate a substituent branching from the inhibitor. Voids within the gorge are displayed in yellow, the solvent-accessible surface of E2020 is in purple, the solvent-accessible surface of the gorge is shown as a brown net, the CPK model of the solvent molecules is in lilac, residues near voids are in light blue, and the catalytic triad is represented by orange sticks.

shown in Figure 7, one can see that most of these waters are conserved (G Koellner, GK, IS, JLS and T Steiner, unpublished results). In the E2020 structure, in fact, only three of the conserved waters seen in the native enzyme are displaced. From this one can conclude that a large ligand, such as E2020, fits into the gorge by displacing primarily the unbound solvent molecules. Many of the conserved waters appear to adhere to the gorge wall and may, perhaps, be considered as an integral part of the structure of the gorge rather than as voids. This may be especially important in relation to drug design (see below), as well as in molecular dynamics studies. It should also be noted that water molecules not observed in the native structure are seen in the E2020 complex, where they bridge between the inhibitor and the enzyme. Specifically WAT 1159, WAT 1160 and WAT 1254 (see Figure 5) are 'novel' structured waters not previously seen in the native structure, while five ordered waters in the native structure are displaced.

Structure-based modification of E2020

Chemical modification of an already effective drug can often improve its pharmacological profile in terms of affinity and specificity. The calculated 'empty' spaces within

the gorge (see Figures 4 and 8), which are revealed in the 3D structure of the E2020–AChE complex, point to candidate sites on the inhibitor where added functions might indeed enhance its pharmacological profile. Separation of enantiomers, which are chemically indistinguishable by non-chiral environments, is difficult, inefficient and costly. In the case of E2020, we suggest that introduction of a second chiral center, with concomitant generation of a diastereomer system, would facilitate isolation of an active component from the mixture so generated [42,43]. Inspection of the empty spaces left within the aromatic gorge by the ordered solvent and by E2020 reveals a finger-shaped void at the acyl-binding pocket. This pocket, defined by Phe288, Phe290, Phe331 and Trp233, could envelop a non-polar substituent branching from the piperidine ring at position E2020 C12. Such a substitution, which would fit into the 'acyl pocket', combined with the existing chiral center, would produce a separable diastereomeric inhibitor.

The recent observations concerning the effect of peripheral-site ligands on AChE-enhanced amyloid deposition [10], mentioned above, raise the possibility that E2020, which our data clearly show as stacking against Trp279, might also moderate the rate of fibril formation. Many of the compounds synthesized and tested by the Eisai company involved modification of this segment of the molecule [15,16]. Nevertheless, it should be borne in mind that the screening that they carried out involved assessment of affinity for AChE, together with selectivity for AChE relative to BChE, but not a possible effect on amyloid fibril assembly or deposition.

Biological implications

Acetylcholinesterase (AChE), the enzyme that hydrolyzes the neurotransmitter acetylcholine (ACh) at cholinergic synapses [44], is the target of the first generation of drugs for the treatment of Alzheimer's disease. E2020 is the second drug targeted at AChE approved for use by the FDA for treatment of this condition. As design and development of the drug preceded the determination of the 3D structure of AChE, it was of interest to use X-ray crystallography to clearly delineate the structural factors governing its selectivity and specificity. This was particularly important because E2020 bears no structural resemblance to other anticholinesterase drugs either approved or under advanced clinical trial, such as tacrine, huperzine A and ENA-713 [45]. Our study shows, *a posteriori*, that the design of E2020 took advantage of several important features of the active-site gorge of AChE to produce a drug with both high affinity and a high degree of selectivity for the enzyme, but not for butyrylcholinesterase (BChE). The high affinity results from interaction of E2020 with the aromatic residue involved in recognition of ACh at the bottom of the gorge, Trp84, with a second aromatic residue at the midpoint of the gorge, Phe330, and with a third residue, Trp279, which is part of the peripheral

anionic site at the top of the gorge. The fact that these two latter residues are conserved in AChE, but absent in BChE, leads to the selectivity that may be an important clinical consideration, as inhibition of BChE may cause potentiating site effects. Our study also delineates voids within the gorge of AChE that are not occupied by E2020, which could serve as sites for modification of E2020 to produce drugs with greater affinity and/or selectivity for AChE. It is worth noting that the 3D structure of *Torpedo californica* AChE (*TcAChE*) is very similar to those of both mouse [46] and human AChE [47]. Thus, the conclusions drawn from the structure of the E2020-*TcAChE* complex should be valid for the mammalian enzyme.

Finally, analogs of E2020 are under consideration as a possible new class of insecticides [48]. The structure of *Drosophila* AChE has recently been solved to 2.7 Å resolution in our laboratory [49] (M Harel, GK, H Greenblatt, L Toker, W Mallender, TL Rosenberry, T Lewis, IS and JLS, unpublished results). Although *Drosophila* AChE shares overall structural features with the *Torpedo* and human enzymes, it also displays marked differences. Our combined knowledge of the vertebrate and invertebrate enzymes should be valuable in developing effective insecticides that combine high specificity for the insect enzyme with low toxicity in humans.

Materials and methods

Protein preparation and crystallization

TcAChE was purified and crystallized as described previously [36]. E2020, as the hydrochloride salt of the pure racemate, was a generous gift from Dr BP Doctor (Division of Biochemistry, Walter Reed Army Institute of Research, Washington, DC). *TcAChE* crystals of trigonal morphology were soaked for five days at 4°C in mother liquor (36% PEG 200, 10 mM NaCl, 50 mM MES, pH 5.8) containing ~10 mM (*R,S*) E2020.

X-ray data collection and processing

The X-ray data were collected from a single crystal that was flash cooled in a 100K nitrogen stream after exchanging the exterior solvent drop with a coating of Exxon high viscosity motor oil [50]. Data were collected in-house, at the Weizmann Institute, utilizing a Rigaku RAXIS-II image-plate system, and a Rigaku FR300 X-ray generator employing a copper target set at 50 mA and 50 kV. The data-collection scheme was optimized by use of the software STRATEGY [51], and consisted of 81 frames of 0.5° rotation and 30 min exposure time each. The diffraction data were extracted from the frames using the software package HKL [52], resulting in a 98.1% complete dataset of 34,264 reflections, overall R_{sym} of 5% and overall I/σ ratio 13.8 (see Table 1).

Model refinement and analysis

The structure was refined using the starting model of native *TcAChE* (PDB code 2ACE) with the program X-PLOR version 3.851 [53]. Refinement employed all 30–2.5 Å data. Following overall anisotropic B-factor and bulk-solvent corrections, the structure was first refined as a single rigid body. Subsequently, refinement was carried out on individual atoms, with restraints, using simulated annealing alternating with positional and temperature-factor refinement. The model was fitted to the observed electron density using the software O [54] on a Silicon Graphics workstation. This program was also used to overlay analogous models by least-squares minimization of C α positions. The intermediate and final models were analyzed using the software OOPS [55], PROCHECK [56] and WHATCHECK [57], and corrections to the model based on these

analyses were implemented (see Table 1). Voids of minimal continuous volume of one spherical cubic angstrom were calculated using the software SurfNet [58], between the inhibitor molecule as one entity and the protein and solvent molecules, taken together, as a second entity.

Accession numbers

The PDB code of the E2020-*TcAChE* complex is IEVE.

Acknowledgements

We thank BP Doctor (Walter Reed Army Institute of Research, Washington DC) for generously providing us with E2020, and Terry Lewis (Jealott's Hill Research Station, Zeneca Agrochemicals, Bracknell, UK) and Yoshiyuki Kawakami (Tsukuba Research Laboratories, Eisai Ltd, Tsukuba, Japan) for valuable discussions. This work was supported by the US Army Medical Research Acquisition Activity under Contract No. DAMD17-97-2-7022, the European Union IVth Framework in Biotechnology, the Kimmelman Center for Biomolecular Structure and Assembly, Israel, the Nella and Leon Benozzi Center for Neurosciences, and the generous support of Tania Friedman. IS is Bernstein-Mason Professor of Neurochemistry.

References

- Drachman, D.A. & Leavitt, J. (1974). Human memory and the cholinergic system. *Arch. Neurol.* **30**, 113-121.
- Bowen, D.M., *et al.*, & Davison, A.N. (1983). Biochemical assessment of serotonergic and cholinergic dysfunction and cerebral atrophy in Alzheimer's disease. *J. Neurochem.* **41**, 266-272.
- Bartus, R.T., Dean, R.L., Beer, B. & Lippa, A.S. (1982). The cholinergic hypothesis of geriatric memory dysfunction. *Science* **217**, 408-414.
- Dunnett, S.B. & Fibiger, H.C. (1993). Role of forebrain cholinergic systems in learning and memory: relevance to the cognitive deficits of aging and Alzheimer's dementia. *Prog. Brain Res.* **98**, 413-420.
- Weinstock, M. (1997). Possible role of the cholinergic system and disease models. *J. Neural Transm. Suppl.* **49**, 93-102.
- Becker, R., Giacobini, E., Elble, R., McIlhany, M. & Sherman, K. (1988). Potential pharmacotherapy of Alzheimer's disease. A comparison of various forms of physostigmine administration. *Acta Neurol. Scand. Suppl.* **116**, 19-32.
- Zhang, R.W., *et al.*, & Yang, R.M. (1991). Drug evaluation of huperzine A in the treatment of senile memory disorders. *Acta Pharm. Sinica* **12**, 250-252.
- Weinstock, M., Razin, M., Chorev, M. & Enz, A. (1994). Pharmacological evaluation of phenyl-carbamates as CNS-selective acetylcholinesterase inhibitors. *J. Neural Transm. Suppl.* **43**, 219-225.
- Knopman, D.S. (1998). Metrifonate for Alzheimer's disease: Is the next cholinesterase inhibitor better? *Neurology* **50**, 1203-1206.
- Inestrosa, N.C., *et al.*, & Garrido, J. (1996). Acetylcholinesterase accelerates assembly of amyloid-beta-peptides into Alzheimer's fibrils: possible role of the peripheral site of the enzyme. *Neuron* **16**, 881-891.
- Reyes, A.E., *et al.*, & Inestrosa, N.C. (1997). A monoclonal antibody against acetylcholinesterase inhibits the formation of amyloid fibrils induced by the enzyme. *Biochem. Biophys. Res. Commun.* **232**, 652-655.
- Davis, K.L. & Powchik, P. (1995). Tacrine. *Lancet* **345**, 625-630.
- Nightingale, S.L. (1997). Donepezil approved for treatment of Alzheimer's disease. *JAMA* **277**, 10.
- Kawakami, Y., Inoue, A., Kawai, T., Wakita, M., Sugimoto, H. & Hopfinger, A.J. (1996). The rationale for E2020 as a potent acetylcholinesterase inhibitor. *Bioorg. Med. Chem.* **4**, 1429-1446.
- Cardozo, M.G., Imura, Y., Sugimoto, H., Yamanishi, Y. & Hopfinger, A.J. (1992). QSAR analyses of the substituted indanone and benzylpiperidine rings of a series of indanone-benzylpiperidine inhibitors of acetylcholinesterase. *J. Med. Chem.* **35**, 584-589.
- Cardozo, M.G., Kawai, T., Imura, Y., Sugimoto, H., Yamanishi, Y. & Hopfinger, A.J. (1992). Conformational analyses and molecular-shape comparisons of a series of indanone-benzylpiperidine inhibitors of acetylcholinesterase. *J. Med. Chem.* **35**, 590-601.
- Sussman, J.L., *et al.*, & Silman, I. (1991). Atomic structure of acetylcholinesterase from *Torpedo californica*: a prototypic acetylcholine-binding protein. *Science* **253**, 872-879.
- Rupniak, N.M., Tye, S.J. & Field, M.J. (1997). Enhanced performance of spatial and visual recognition memory tasks by the selective acetylcholinesterase inhibitor E2020 in rhesus monkeys. *Psychopharmacology Berlin* **131**, 406-410.
- Galli, A., Mori, F., Benini, L. & Cacciarelli, N. (1994). Acetylcholinesterase protection and the anti-diisopropylfluorophosphate efficacy of E2020. *Eur. J. Pharmacol.* **270**, 189-193.

20. Thomsen, T. & Kewitz, H. (1990). Selective inhibition of human acetylcholinesterase by galanthamine *in vitro* and *in vivo*. *Life Sci.* **46**, 1553-1558.
21. Loewenstein, Y., Gnatt, A., Neville, L.F. & Soreq, H. (1993). Chimeric human cholinesterase. Identification of interaction sites responsible for recognition of acetyl- or butyrylcholinesterase-specific ligands. *J. Mol. Biol.* **234**, 289-296.
22. Sugimoto, H., Imura, Y., Yamanishi, Y. & Yamatsu, K. (1995). Synthesis and structure-activity-relationships of acetylcholinesterase inhibitors – 1-Benzyl-4-[(5,6-dimethoxy-1-oxoindan-2-yl)methyl]piperidine hydrochloride and related compounds. *J. Med. Chem.* **38**, 4821-4829.
23. Cheng, D.H., Ren, H. & Tang, X.C. (1996). Huperzine A, a novel promising acetylcholinesterase inhibitor. *Neuroreport* **8**, 97-101.
24. Villalobos, A., et al., & Frost White, W. (1995). 5,7-dihydro-3-[2-[1-(phenylmethyl)-4-piperidinyl]ethyl]-6H-pyrrolo[3,2-f]-1,2-benzisoxazol-6-one: a potent and centrally-selective inhibitor of acetylcholinesterase with an improved margin of safety. *J. Med. Chem.* **38**, 2802-2808.
25. Pang, Y.P. & Kozikowski, A.P. (1994). Prediction of the binding site of 1-benzyl-4-[(5,6-dimethoxy-1-indanon-2-yl)methyl]piperidine in acetylcholinesterase by docking studies with the SYSDOC program. *J. Comput. Aided Mol. Des.* **8**, 683-693.
26. Harel, M., et al., & Silman, I. (1992). Conversion of acetylcholinesterase to butyrylcholinesterase: modeling and mutagenesis. *Proc. Natl Acad. Sci. USA* **89**, 10827-10831.
27. Schumacher, M., et al., & Taylor, P. (1986). Primary structure of *Torpedo californica* acetylcholinesterase deduced from its cDNA sequence. *Nature* **319**, 407-409.
28. Harel, M., et al., & Sussman, J.L. (1993). Quaternary ligand binding to aromatic residues in the active-site gorge of acetylcholinesterase. *Proc. Natl Acad. Sci. USA* **90**, 9031-9035.
29. Harel, M., Quinn, D.M., Nair, H.K., Silman, I. & Sussman, J.L. (1996). The X-ray structure of a transition state analog complex reveals the molecular origins of the catalytic power and substrate specificity of acetylcholinesterase. *J. Am. Chem. Soc.* **118**, 2340-2346.
30. Leviit, M. & Perutz, M.F. (1988). Aromatic rings act as hydrogen bond acceptors. *J. Mol. Biol.* **201**, 751-754.
31. Burley, S.K. & Petsko, G.A. (1986). Amino-aromatic interactions in proteins. *FEBS Lett.* **203**, 139-143.
32. Inoue, A., Kawai, T., Wakita, M., Imura, Y., Sugimoto, H. & Kawakami, Y. (1996). The simulated binding of (+/-)-2,3-dihydro-5,6-dimethoxy-2-[(1-(phenylmethyl)-4-piperidinyl)methyl]-1H-inden-1-one hydrochloride (E2020) and related inhibitors to free and acylated acetylcholinesterases and corresponding structure-activity analyses. *J. Med. Chem.* **39**, 4460-4470.
33. Verdonk, M.L., Boks, G.J., Kooijman, H., Kanters, J.A. & Kroon, J. (1993). Stereochemistry of charged nitrogen-aromatic interactions and its involvement in ligand-receptor binding. *J. Comput. Aided Mol. Des.* **7**, 173-182.
34. Dougherty, D. (1996). Cation- π interactions in chemistry and biology: A new view of benzene, Phe, Tyr, and Trp. *Science* **271**, 163-168.
35. Biosym (1993). InsightII. Biosym Technologies San Diego.
36. Raves, M.L., Harel, M., Pang, Y.P., Silman, I., Kozikowski, A.P. & Sussman, J.L. (1997). Structure of acetylcholinesterase complexed with the nootropic alkaloid, (-)-huperzine A. *Nat. Struct. Biol.* **4**, 57-63.
37. Shafferman, A., et al., & Ariel, N. (1992). Substrate inhibition of acetylcholinesterase: residues affecting signal transduction from the surface to the catalytic center. *EMBO J.* **11**, 3561-3568.
38. Ordentlich, A., et al., & Shafferman, A. (1993). Dissection of the human acetylcholinesterase active center determinants of substrate specificity. Identification of residues constituting the anionic site, the hydrophobic site, and the acyl pocket. *J. Biol. Chem.* **268**, 17083-17095.
39. Radic, Z., Pickering, N.A., Vellom, D.C., Camp, S. & Taylor, P. (1993). Three distinct domains in the cholinesterase molecule confer selectivity for acetyl- and butyrylcholinesterase inhibitors. *Biochemistry* **32**, 12074-12084.
40. Antosiewicz, J., Wlodek, S.T. & McCammon, J.A. (1996). Acetylcholinesterase: role of the enzyme's charge distribution in steering charged ligands toward the active site. *Biopolymers* **39**, 85-94.
41. Zhou, H.X., Wlodek, S.T. & McCammon, J.A. (1998). Conformation gating as a mechanism for enzyme specificity. *Proc. Natl Acad. Sci. USA* **95**, 9280-9283.
42. Shah, R.R. (1993). Clinical pharmacokinetics: current requirements and future perspectives from a regulatory point of view. *Xenobiotica* **23**, 1159-1193.
43. Nation, R.L. (1989). Enantioselective drug analysis: problems and resolutions. *Clin. Exp. Pharmacol. Physiol.* **16**, 471-477.
44. Barnard, E.A. (1974). Neuromuscular transmission – enzymatic destruction of acetylcholine. In *The Peripheral Nervous System*. (Hubbard, J.I., ed.), pp. 201-224, Plenum, NY.
45. Baron, P., Harel, M., Millard, C., Enz, A., Sussman, J.L. & Silman, I. (1998). Kinetic and X-ray crystallographic studies of the binding of ENA-713 to *Torpedo californica* acetylcholinesterase (TcAChE). In *Structure and Function of Cholinesterases and Related Proteins*. (Doctor, B.P., Quinn, D.M., Rotundo, R.L. & Taylor, P., eds), pp. 373-374, Plenum, NY.
46. Bourne, Y., Taylor, P., Kanter, J.R., Bougis, P.E. & Marchot, P. (1998). Crystal structure of mouse acetylcholinesterase. In *Structure and Function of Cholinesterases and Related Proteins*. (Doctor, B.P., Quinn, D.M., Rotundo, R.L. & Taylor, P., eds), pp. 315-322, Plenum, NY.
47. Kryger, G., et al., & Sussman, J.L. (1998). 3D structure of a complex of human recombinant acetylcholinesterase with fasciculin-II at 2.7 Å resolution. In *Structure and Function of Cholinesterases and Related Proteins*. (Doctor, B.P., Quinn, D.M., Rotundo, R.L. & Taylor, P., eds), pp. 323-326, Plenum, NY.
48. Greenblatt, H., et al., & Sussman, J.L. (1998). Crystal structures of complexes of E2020 related compounds with *Torpedo* acetylcholinesterase. In *Structure and Function of Cholinesterases and Related Proteins*. (Doctor, B.P., Quinn, D.M., Rotundo, R.L. & Taylor, P., eds), p. 371, Plenum, NY.
49. Kryger, G., et al., & Harel, M. (1998). Structural studies on human and insect acetylcholinesterase. *Abstract from the Sixth International Meeting on Cholinesterases*, La Jolla, CA, p. 14.
50. Hope, H. (1988). Cryocrystallography of biological macromolecules: a generally applicable method. *Acta Crystallogr. B* **44**, 22-26.
51. Ravelli, R.B.G., Sweet, R.M., Skinner, J.M., Duisenberg, A.J.M. & Kroon, J. (1997). STRATEGY: a program to optimize the starting spindle angle and scan range for X-ray data collection. *J. Appl. Crystallogr.* **30**, 551-554.
52. Otwinowski, Z. (1993). Oscillation data reduction program. In *Proceedings of the CCP4 Study Weekend: Data Collection and Processing*. (Sawyer, L., Isaacs, N. & Bailey, S., eds), pp. 56-62, SERC, Daresbury.
53. Brünger, A.T., Kuriyan, J. & Karplus, M. (1987). Crystallographic R factor refinement by molecular dynamics. *Science* **235**, 458-460.
54. Jones, T.A., Zou, J.Y., Cowan, S.W. & Kjeldgaard, M. (1991). Improved methods for the building of protein models in electron density maps and the location of errors in these models. In *Crystallographic Computing*. (Moras, D., Podany, A.D. & Thierry, J.C., eds), pp. 413-432, Oxford Univ. Press, Oxford.
55. Kleywegt, G.J. & Jones, T.A. (1996). Efficient rebuilding of protein structures. *Acta Crystallogr. D* **52**, 829-832.
56. Laskowski, R.A., MacArthur, M.W., Moss, D. & Thornton, J.M. (1993). PROCHECK: a program to check the stereochemical quality of protein structures. *J. Appl. Crystallogr.* **26**, 283-291.
57. Vriend, G. (1990). WHAT IF: a molecular modelling and drug design program. *J. Mol. Graph.* **8**, 52-56.
58. Laskowski, R.A. (1995). SURFNET: a program for visualizing molecular surfaces, cavities and intermolecular interactions. *J. Mol. Graph.* **13**, 323-330.